

Reflectivity Function based Illumination and Sensor Planning for Industrial Inspection

Marc M. Ellenrieder, Christian Wöhler and Pablo d'Angelo ^a

^aDaimlerChrysler AG, Research & Technology, REI/AI, P.O. Box 2360, 89013 Ulm, Germany

ABSTRACT

In this paper, we will derive a phenomenological model of the bidirectional reflectance distribution function of non-LAMBERTIAN metallic materials typically used in industrial inspection. We will show, how the model can be fitted to measured reflectance values and how the fitted model can be used to determine a suitable illumination position. Together with a given sensor pose, this illumination position can be used to calculate the necessary shutter time, aperture, focus setting and expected gray value to successfully perform a given visual inspection task. The paper concludes with several example inspection tasks.

Keywords: automatic illumination positioning, bidirectional reflectance distribution function, non-Lambertian surfaces, internal sensor settings, visibility map, inspection, task planning

1. INTRODUCTION AND MOTIVATION

Automation of visual inspection tasks is an important field of current research in industrial machine vision. Some of the key issues for a successful inspection process are suitable positions for the cameras and illumination devices. While several approaches for automatic sensor planning are available,¹⁻³ interaction between illumination, inspected object and sensor settings is considered only by very few publications. Some approaches, e.g. the one presented by Khawaja et al.,⁴ use certain assumptions to determine the position of lighting devices and do not model the interaction between light, surface and sensor in a thorough manner. Another publication by Cowan and Kovcsi⁵ calculates approximate regions of acceptable light locations (in terms of the dynamic range of the used sensor) of single points on flat surfaces with pure LAMBERTIAN reflection in case of telecentric lenses and point light sources. Additionally, Cowan and Kovcsi⁵ calculate the region where specular reflections might occur. However, they present no solution for complex surfaces and no treatment of more complex lighting criteria, such as maximizing the contrast between certain surfaces. To our knowledge, no publication derives a physical reflection model of the inspected material and uses it to calculate the amount of light received by the sensor. However, several settings of the camera, such as aperture and shutter time, directly depend on the amount of received light energy per pixel. Others, such as depth of field, indirectly depend on the received energy: low illumination levels generally require larger apertures and result in less depth of field. For inspection of several regions on highly non-planar objects this might e. g. imply the need for an additional camera for correct inspection.

The amount of received light energy per pixel directly depends on the bidirectional reflectance distribution function (BRDF) of the surface material of the inspected object and its geometry. While the latter is generally available through CAD models, reflectivity functions of arbitrary materials are often difficult to obtain. In this paper, we will present a method to measure the BRDF of arbitrary materials. We will show how the reflectivity function can be used to derive the absolute amount of energy per pixel a camera receives. For several metallic materials common to industrial machine vision, we will show how to fit a reflectivity function model similar to the one described by Nayar et al.⁶ to the measured data.

We will then show how to extend an existing framework for automatic viewpoint selection³ to illumination planning. In this system, visibility of an inspected region of interest is determined by a spherical visibility map. We will show how to map the measured BRDF on the visibility map and derive a scalar cost function whose minimum determines a three-dimensional illumination position, from which a previously located sensor receives a desired amount of light energy. At the same time, the approach guarantees that the inspected areas are evenly illuminated resulting in optimal contrast. Additionally, we will show how to determine the internal settings of the sensor such as aperture, gain, and shutter time for appropriate exposure and depth of field. The system is evaluated based on several real inspection tasks from current production processes.

Contact Author's EMail: Marc.Ellenrieder@DaimlerChrysler.Com

2. AUTOMATIC OPTIMAL VIEWPOINT PLANNING FOR INDUSTRIAL INSPECTION

In a previous publication,³ we have shown how to calculate one or more optimal viewpoints given a geometric description of the inspected object, the location of two-dimensional feature areas that are to be inspected and a description of the sensor. However, illumination, its interaction with the inspected object and its influence on the internal sensor settings was not considered. Before we address these issues in this paper, some central concepts of the viewpoint planning system need to be presented.

2.1. Viewpoint Requirements and Cost Functions

In our viewpoint planning system, a feature F is a two-dimensional area on the surface of an object. Each feature is to be inspected with a specific image processing algorithm, e.g. barcode reading algorithm, shape reconstruction from shading, or other methods. In order to function, these algorithms have specific requirements: a required minimum resolution, a necessary viewing angle, etc. Any viewpoint from which the inspection task can be performed must fulfill these requirements. Therefore, we call these requirements *viewpoint requirements*. In our existing framework,³ a viewpoint $\tilde{\omega}$ is considered to be a six-dimensional pose vector of the sensor.

Automatic viewpoint planning systems need a means to compare different viewpoints. For this, we have shown how to express any combination of viewpoint requirements as a convex function. The global minimum of this convex function, found by a numerical optimization scheme, is considered to be the optimal viewpoint. To guarantee fast convergence, we chose exponential functions of the type

$$f_{\max} = \exp\left(\frac{x}{x_{\max}} - 1\right) \text{ and } f_{\min} = \exp\left(\frac{-x}{x_{\min}} + 1\right) \quad (1)$$

for viewpoint requirements that require a minimum or maximum value. Without loss of generality, we define a function value of 1 to be the highest acceptable value of a viewpoint requirement function.

2.2. Feature Visibility

Obviously, for any visual inspection feature visibility is the most important viewpoint requirement. In our system, we use a spherical *visibility map* as a means to determine feature visibility. In principle, a visibility map is defined for points on the surface of an object. It is calculated by projecting the inspected object (and possibly the whole scene) onto a unit sphere centered at the point on the object for which the map is calculated. The unit sphere is then sampled at constant azimuth / elevation intervals and the boolean information whether something has been projected on the current point on the sphere or not, is transcribed into a matrix called visibility map. The notion of visibility maps can be extended to two-dimensional areas, if it is assumed that the camera is far away at distance in comparison to the maximum extension (i.e. the length of the longest eigenvector) of the feature. In our existing viewpoint planning framework, visibility maps are also used to calculate a suitable sensor-feature association, so that the object can be inspected with a minimum number of sensors.

Sometimes, it can be useful to quickly determine viewing directions where the visibility of features is as stable as possible towards slight viewpoint deviations. This means that the sensors should be positioned as far away as possible from the occlusion-zone boundaries. One way to achieve this is to calculate the distance transform of a visibility map. However, since visibility maps are spherical projections, we need to use a spherical rather than an Euclidean distance measure. Using the Haversine function $h(x) = \sin^2(x/2)$, the distance of two points $p_1 = (\theta_1, \phi_1)$ and $p_2 = (\theta_2, \phi_2)$ in the visibility map can be expressed as

$$d(p_1, p_2) = 2 \cdot \arctan 2 \left(\sqrt{a}, \sqrt{1-a} \right), \quad (2)$$

where

$$a = h(\theta_2 - \theta_1) + \cos(\theta_1) \cos(\theta_2) h(\phi_2 - \phi_1). \quad (3)$$

By convention, we define $d < 0$ for visible viewing directions and $d > 0$ for occluded directions. An extensive description of further visibility map properties along with several application examples can be found in our pertinent publication.⁷

2.3. Incorporating Illumination Planning

In the remainder of this paper, we are going to present an extension of our automatic viewpoint planning framework. We are going to model the interaction of illumination, object material, and sensor settings (shutter time, aperture and focus setting) as convex functions. We assume that the optimal viewpoints have been previously calculated using the automatic viewpoint planning system by Ellenrieder and Komoto.³

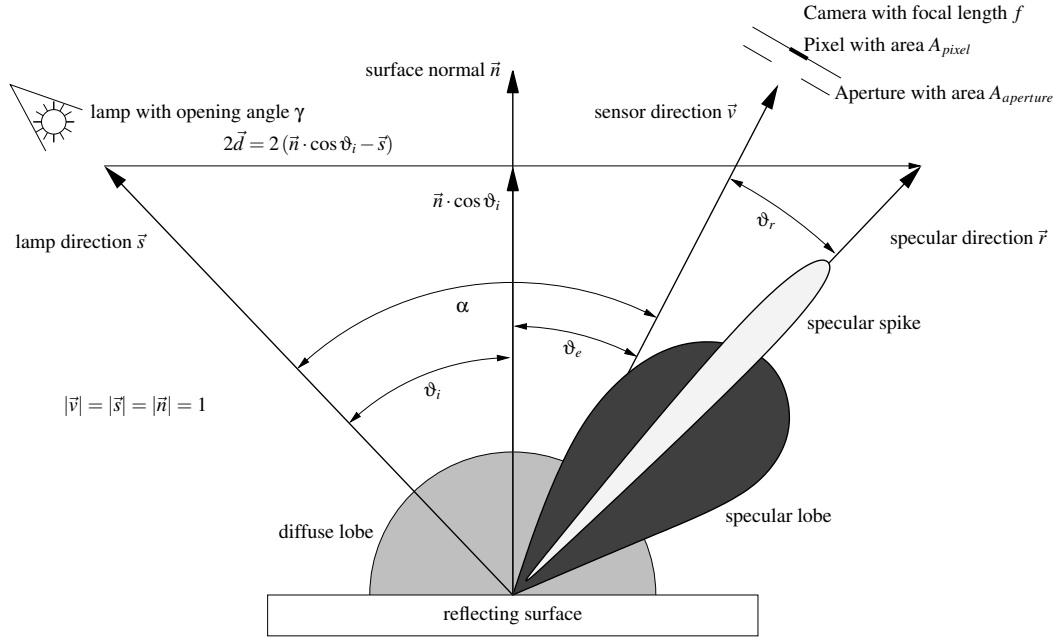


Figure 1. Phenomenological description of the BRDF of non-LAMBERTIAN materials according to Nayar et.al.⁶

3. DESCRIBING SURFACE REFLECTANCE

The key to successful illumination planning is understanding the interaction between light, inspected surface, and sensor. To describe this interaction physically, the surface reflectance of the inspected material is needed. Surface reflectance is known for some materials, especially from the photogrammetric domain. There, most of the time it is assumed that the surface brightness is independent of the sensor position. The reflectance of such material is called diffuse or LAMBERTIAN. Many materials common to industrial machine vision, however, are far from showing a LAMBERTIAN reflectance. Their reflectance function is dependant on the angles between sensor, surface normal, and illumination device. Since the exact relations for a given material are generally not available, one needs to derive a phenomenological model of the reflectance and estimate the model parameters to match with the measured reflectance. In the following, we are going to present such a model, measure the actual reflectance of four metallic materials common to industrial production, and fit the measured data to the presented model.

3.1. Modeling the Bidirectional Reflectance Distribution Function

The bidirectional reflectance distribution function (BRDF) of a medium is defined as the ratio of the radiance (brightness) scattered by a surface into a given direction to the collimated power incident on a unit area of the surface.⁸ According to Nayar et al.,⁶ the BRDF of non-LAMBERTIAN surfaces can be modelled as a function with a diffuse (LAMBERTIAN) component, a specular lobe and a specular spike (Fig. 1). This fact can be modeled phenomenologically as follows:

Suppose, the light emitted by the lamp in unit direction \vec{s} is reflected by the surface with unit normal vector \vec{n} into a specular direction \vec{r} , where

$$\vec{r} = \vec{s} + 2\vec{d}, \text{ and} \quad (4)$$

$$\vec{d} = \vec{n} \cos \vartheta_i - \vec{s}. \quad (5)$$

From geometrical optics, it follows that vectors \vec{s} , \vec{r} , and the camera direction unit vector \vec{v} are coplanar. Hence, we can formulate Nayar's reflection model as

$$R = \rho \left(\underbrace{\cos \vartheta_i}_{\text{diffuse}} + \underbrace{\sigma_1 \cos^{m_1} \vartheta_r}_{\text{specular lobe}} + \underbrace{\sigma_2 \cos^{m_2} \vartheta_r}_{\text{specular spike}} \right), \quad (6)$$

with, by convention, $m_2 > m_1$. Similarly to other reflectance distributions, the factor ρ denotes the surface albedo. Using equations (4) and (5), this can be rewritten as

$$R = \rho \left(\cos \vartheta_i + \sum_{i=1}^2 \sigma_i \langle \vec{v}, \vec{r} \rangle^{m_i} \right) = \rho \left(\cos \vartheta_i + \sum_{i=1}^2 \sigma_i (2 \cdot \langle \vec{v}, \vec{n} \rangle \cos \vartheta_i - \langle \vec{v}, \vec{s} \rangle)^{m_i} \right)$$

$$R(\vartheta_i, \vartheta_e, \alpha) = \rho \left(\cos \vartheta_i + \sum_{i=1}^2 \sigma_i (2 \cos \vartheta_e \cos \vartheta_i - \cos \alpha)^{m_i} \right). \quad (7)$$

In photogrammetry, the angle α is called *phase angle*.

3.2. Measuring the bidirectional reflectance distribution

Since the bidirectional reflectance distribution is material specific and is difficult to obtain, we measured the BRDF of four different materials: gray cast iron, sheet metal (steel), gray cast aluminium, and milled aluminium. For this purpose we mounted plane material samples at the center of rotation of a goniometer, focused the camera onto the sample and measured the mean grayvalues received at a known shutter time by the camera in a 17x17 pixel area on the sample for various phase angles α over a ϑ_i and ϑ_e interval of about 90° , respectively. For reasons of symmetry, the remaining angular intervals on the unit sphere do not need to be measured.

3.3. Fitting the BRDF parameters

The measured grayvalues were used to estimate the parameters σ_1 , σ_2 , m_1 and m_2 of eq. (7) in a least-mean-square fitting process at various phase angles α . For this purpose we used a NEWTON-RAPHSON algorithm. The elements of the necessary Jacobian are given by

$$\frac{\partial R}{\partial \sigma_i} = (2 \cos \vartheta_e \cos \vartheta_i - \cos \alpha)^{m_i}, \text{ and} \quad (8)$$

$$\frac{\partial R}{\partial m_i} = \sigma_i (2 \cos \vartheta_e \cos \vartheta_i - \cos \alpha)^{m_i} \cdot \ln(2 \cos \vartheta_e \cos \vartheta_i - \cos \alpha). \quad (9)$$

The parameter ρ , i.e. the surface albedo, translates the phenomenologic model into absolute reflectance values. In the next section, we will show how ρ can be estimated directly.

4. ILLUMINATION INFLUENCE ON THE SENSOR SETTINGS

4.1. Gray Value

The gray value G of a camera-pixel is directly depending on the received energy per pixel P_{pixel} and the shutter time t . From the characteristic curve of the camera, we obtain

$$G = c \cdot P_{\text{pixel}} \cdot t \quad (10)$$

if we assume its response to be linear. Ideally, c is known from the chip manufacturer. However, if this information is not available, it can be estimated by measuring the resulting gray values, if the sensor is illuminated by a laser with known power at different shutter times. The camera used throughout this paper had a slope of $c = 1.5 \cdot 10^{16} \text{ W}^{-1} \text{ s}^{-1}$.

The received energy per pixel P_{pixel} can be calculated as follows: A point light source with an emitting light power of P_L and reflector opening angle γ produces a power density of

$$\Phi_i = P_L \cdot \frac{1}{2\pi(1 - \cos \frac{\gamma}{2}) d_i^2} \left[\frac{W}{m^2} \right] \quad (11)$$

at a distance of d_i to the reflecting surface. This power density hits the reflecting surface area A at an angle ϑ_i . Suppose, on A there are N surface elements, so that each element has an area of $A_p = A/N$ and receives a power of

$$P = \frac{A \cdot \Phi_i \cdot \cos \vartheta_i}{N} [W]. \quad (12)$$

Similarly, the number of surface elements that are projected by the sensor at distance d_k onto a pixel with active area A_{pixel} is given by

$$n_p = \frac{A_{\text{pixel}} d_k^2 N}{f^2 A \cdot \cos \vartheta_e}. \quad (13)$$

Here, f is the focal length of the sensor. Using the bidirectional reflectance function R of the material, eq. (6), and eq. (12), we can calculate the amount of power emitted by a surface element as

$$P_e = \frac{A \cdot \Phi_i}{N} \cdot R. \quad (14)$$

Thus, each pixel receives an effective power of

$$\frac{P_e \cdot \cos \vartheta_e}{2\pi d_k^2} \cdot A_{\text{aperture}} \quad (15)$$

Here, A_{aperture} is the area of the lens' aperture κ given by

$$A_{\text{aperture}} = \frac{\pi f^2}{4\kappa^2}. \quad (16)$$

From eqs. (13) and (15) we can finally calculate the total power P_{pixel} of light received by a pixel:

$$P_{\text{pixel}} = \frac{A_{\text{pixel}} \cdot A_{\text{aperture}} \cdot \Phi_i \cdot R}{2\pi f^2} = \frac{A_{\text{pixel}} \cdot \Phi_i \cdot R}{\underline{\underline{8\kappa^2}}} [W]. \quad (17)$$

Once P_{pixel} has been calculated, we can directly compute the resulting gray value from the characteristic curve, eq. (10).

4.2. Estimating surface albedo ρ

That said, we can now estimate the remaining parameter of the BRDF: the surface albedo ρ . The angles, shutter time, and gray values measured for direct specular reflection, i.e. $\vartheta_r = 0$ and $\vartheta_i = \alpha/2$, are known from sec. 3.2. Hence, using eqs. (6) and (17) we get

$$R = \frac{A_{\text{pixel}} \cdot \Phi_i \cdot P_{\text{pixel}}}{8\kappa^2} = \rho \left(\cos \frac{\alpha}{2} + \sigma_1 + \sigma_2 \right), \quad (18)$$

and thus

$$\rho = \frac{A_{\text{pixel}} \cdot \Phi_i \cdot P_{\text{pixel}}}{8\kappa^2 \left(\cos \frac{\alpha}{2} + \sigma_1 + \sigma_2 \right)}. \quad (19)$$

In our experiments, we found that ρ is – at least for the measured metallic materials – dependant on the phase angle, i.e. $\rho = \rho(\alpha)$. Figure 2 shows the BRDF parameters for four metallic materials that have been estimated using the above methods.

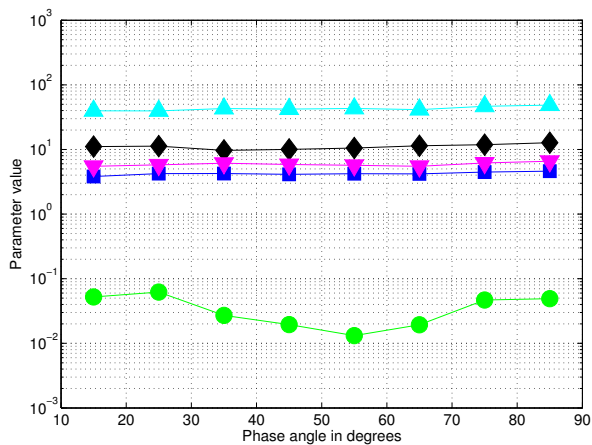
4.3. Depth of field

The internal camera aperture κ and shutter time t are dependant of the received energy per pixel. At the same time, aperture influences the depth of field, i.e. the zone where objects are well focused. Depth of field is generally defined as the difference between a far distance d_f and a near distance d_n . Objects situated at a distance between d_f and d_n are considered well focused.⁹ It is known from technical optics that

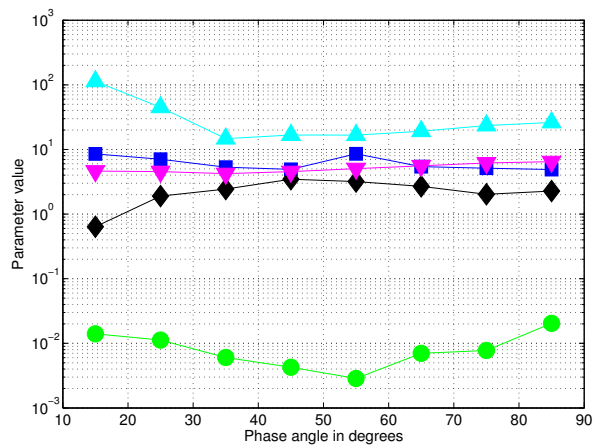
$$d_n = d_n(g, \kappa) = \frac{f^2 \cdot g}{f^2 - \kappa \cdot \sigma (g + f)} \quad (20)$$

$$d_f = d_f(g, \kappa) = \frac{f^2 \cdot g}{f^2 + \kappa \cdot \sigma (g + f)} \quad (21)$$

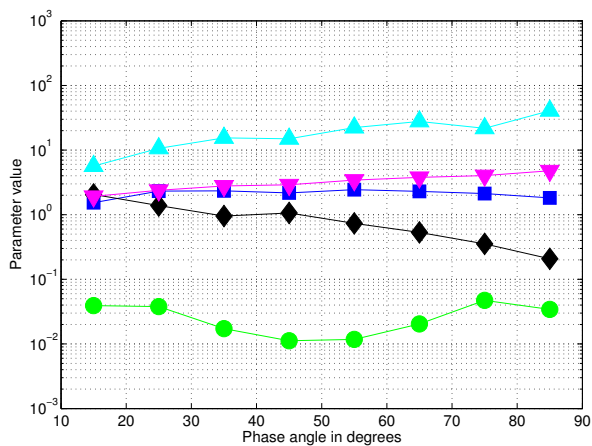
Here, g determines the focus setting of the camera lens and σ is an empirically determined parameter depending on the size of the sensor chip, the diameter of the circle of confusion.⁹ For typical industrial sensors with 1/3" CCD-chips, σ results to $5.015 \cdot 10^{-6} m$.



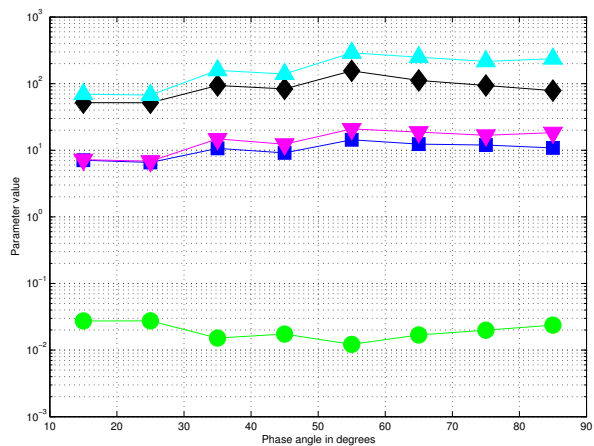
(a) Sheet metal



(b) Gray cast iron



(c) Cast aluminium



(d) Milled aluminium

Figure 2. Fitted BRDF parameters for four typical metallic materials. The parameters of eq. (6), ρ (\bullet), σ_1 (\blacksquare), σ_2 (\blacklozenge), m_1 (\blacktriangledown), and m_2 (\blacktriangle), are plotted for various phase angles α .

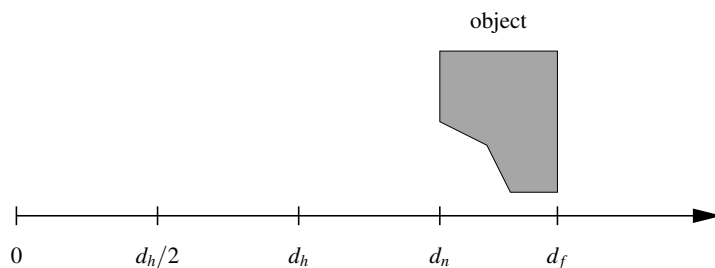


Figure 3. Depth of field

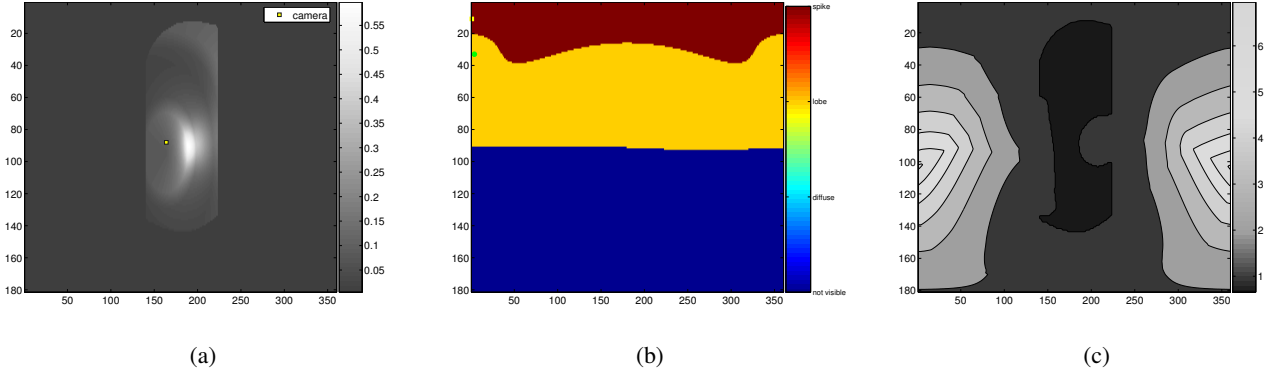


Figure 4. The BRDF of sheet metal mapped onto a visibility map (a), its segmented version (b), and the exponential cost function to keep the lamp inside the region where the lobe is constant (c). In (a) and (b), the direction of the camera is marked by a rectangle.

5. ILLUMINATION PLANNING AS AN OPTIMIZATION PROBLEM

Up to now, we have shown how the material’s bidirectional reflectance function and the light position influence the sensor settings. These results can now be used to express the illumination planning problem as a convex optimization problem similar to eq. (1). We have identified four particular illumination requirements:

- the resulting grayvalues should be in a inspection-task-specific interval,
- a small change in the illumination position must not change the resulting grayvalue,
- the depth of field and thus the aperture needs to be sufficient for correct inspection, and
- the sensor settings (shutter time, aperture, and focus setting) need to be well within the limits of the sensor.

In the following, we will describe how to express these requirements as convex cost functions dependant on the shutter time t , aperture κ , focus setting g , and lamp position \vec{s} .

5.1. Cost Function for Resulting Gray Values, Depth of Field and Sensor Limits

Using equations (10) and (17) we can directly calculate the resulting gray value on the sensor. If the minimally and maximally allowed gray values G_{\min} and G_{\max} are given, the necessary cost function can be directly modeled using eq. (1). Similarly, we define cost functions for the minimum and maximum required depth of field, eqs. (20) and (21), and the limits of the sensors.

5.2. Cost Function for Regions of Similar Brightness

By definition, the BRDF describes the radiance (brightness) reflected by a material into a given direction.⁸ If we calculate the dominant term of eq. (6), i.e. diffuse component, specular lobe, or specular spike, for that direction, we can safely assume that a lamp situated in said direction will result in a certain type of reflection. If we map the type of the dominant term onto the visibility map of a feature area, this results in a “region-of-similar-brightness-map”. An inspection algorithm might require a particular type of reflection component: e.g. diffuse reflection for shape from shading or specular reflection for shape from polarization. In order to keep the illumination well inside the required reflection type, we calculate a distance transform of the segmented reflectance map using eq. (2) and use the distance as the argument of an exponential function similar to eq. (1). Hence, we get a requirement cost of 1 at the border of the region of similar brightness, and well above 1 elsewhere. Figure 4 shows the reflectance function of sheet metal mapped onto a visibility map, the segmented reflectance map and the cost function using a distance transform of the region where the specular lobe is dominant.

5.3. Overall Cost Function

In order to guarantee optimal convergence, we need to combine the particular requirement functions into a global cost function. At the same time, we want to make sure, that – once the minimum of the global cost function has been found – all of our requirements are automatically met, i.e. all have a function value < 1 . For this, we use the *log-sum-exponential* function

$$g(\vec{x}) = \ln \left(\sum_{i=1}^N e^{x_i} \right). \quad (22)$$

It is known to be convex for all $\vec{x} = (x_1, \dots, x_N) \in \mathbb{R}^N$. Equation (22) can be interpreted as a differentiable and, in fact, analytic approximation of the *max* function, since

$$\max \{x_1, \dots, x_N\} \leq \ln \left(\sum_{i=1}^N e^{x_i} \right) \leq \max \{x_1, \dots, x_N\} + \ln N \quad (23)$$

for all N .¹⁰ It is also known from convex optimization theory, that

$$f(\vec{x}) = g(\vec{h}(\vec{x})) \quad \vec{x}, \vec{h} \in \mathbb{R}^N, g \in \mathbb{R} \quad (24)$$

is convex, if both g and \vec{h} are strictly convex on \mathbb{R} and \mathbb{R}^N , respectively. This fact is of importance for the proposed optimal viewpoint calculation framework. Equations (22), (23), and (24) enable us to express the problem of finding an optimal illumination position, i.e. an illumination position fulfilling all requirements, as a parameter-free convex optimization problem that is known to have a unique minimum. Consequently, if eq. (22) is minimized and

$$f_{\min} - \ln N \leq 1 \quad (25)$$

we have inherently shown that no component of \vec{x} is larger than 1 and thus all viewpoint requirements are met.

5.4. Initialization and Final Optimization

We have now modeled the task of finding an optimal illumination position as a convex optimization problem. The overall cost function can be minimized using any standard numerical minimization method. In order to guarantee fast convergence, we have chosen the initial values of the optimization parameters using the following heuristics:

The initial focus setting g_{init} and aperture κ_{init} are chosen such that the feature areas inspected by the camera are well within the depth of field of the lens. The initial position of the illumination device \vec{s}_{init} is set to be the same as the position of the camera. The remaining shutter time t_{init} is calculated such that – while using g_{init} , \vec{s}_{init} , and κ_{init} as parameters for eqs. (10) and (17) – a medium gray value of 128 is expected. Final minimization of the overall cost function is finally done using a standard SIMPLEX algorithm.

6. EXPERIMENTAL INVESTIGATIONS

The presented framework was evaluated on several inspection tasks. The optimum sensor position for each inspection task was calculated using the existing viewpoint planning framework described by Ellenrieder and Komoto.³ The employed 8-bit camera had a resolution of 1032x776 pixel at a focal length of 25 mm. For all experiments, we used LED illumination with an effective light power of 230.43 mW and reflector opening angle of $\gamma = 12^\circ$. The necessary grayvalue interval for successful inspection was 110-150.

In the first example, parts of a connection rod made out of gray cast metal was inspected. The optimum camera position calculated by our viewpoint planning system was at a distance of 35 cm nearly perpendicular above the part (fig. 5a). Using the above described framework, we calculated an optimal lamp position at a phase angle of 12° at a distance of 40 cm (fig. 5b). To guarantee a necessary depth of field, we computed an aperture of 6.2. It can be seen in fig. 5c, that the resulting image taken by the camera at a shutter speed of 11.7 ms has a mean grayvalue of 130.

In the second example, the surface of an aluminium hinge was inspected (fig 6). Here, the optimum camera position was at a distance 50 cm nearly perpendicular above the part. The estimated optimal lamp position resulted to a distance of 25.8 cm at a phase angle of about 28.9° . The necessary aperture and shutter time for a desired gray value range of 100-125 were computed as $\kappa = 5.6$ and $t = 11.6 \text{ ms}$, respectively. The measured mean gray value was found to be 120.

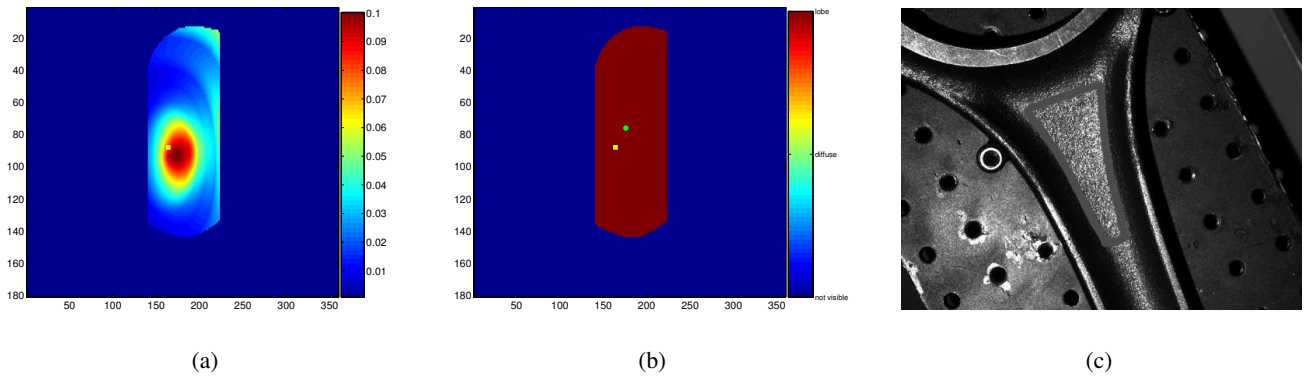


Figure 5. Inspection of a connection rod. Visibility map with mapped BRDF (a) . The camera direction is marked with a bright rectangle. Segmented reflectance map (b); the lamp position is marked with a bright point. (c) Actual image taken by the camera. The marked region indicates where the inspection task was performed.

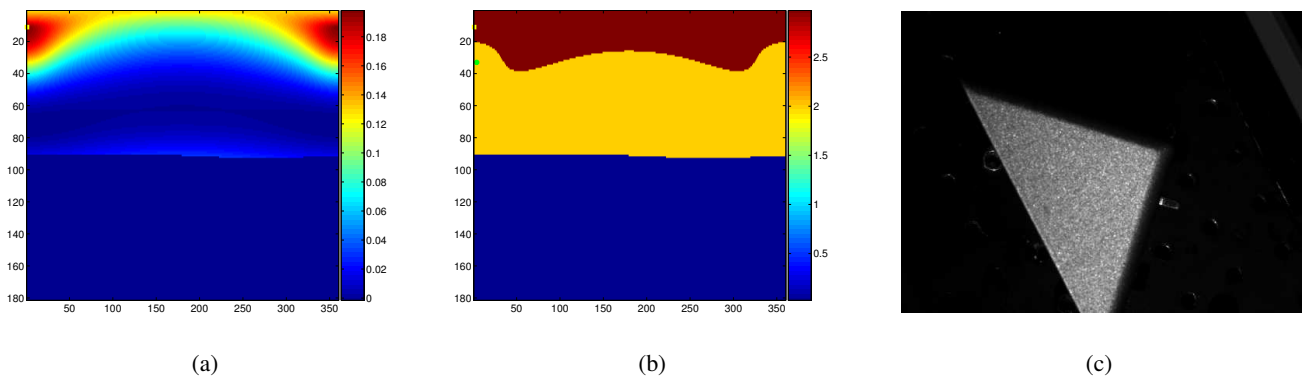


Figure 6. Inspection of an aluminium hinge. Visibility map with mapped BRDF (a) . The camera direction is marked with a bright rectangle in the upper left corner. Segmented reflectance map (b); the lamp position inside the lobe region is marked with a bright point. (c) Actual image taken by the camera.

7. SUMMARY AND CONCLUSION

In this paper, we have demonstrated how the bidirectional reflectance distribution function (BRDF) of non-LAMBERTIAN materials can be modeled. We have measured the BRDF of four typical metallic materials – sheet metal (steel), gray cast iron, gray cast aluminium, and milled aluminium – using a goniometer setup. The measured reflectance values have been fitted to a mathematical model of the BRDF. Using these parameters, we have shown how to derive the absolute amount of energy per pixel a camera receives, if aperture and shutter time are known. We have then extended an existing framework for automatic viewpoint selection³ to illumination planning by mapping the measured BRDF on the visibility map. Using this reflectance map a scalar cost function whose minimum determines an optimal three-dimensional illumination position was derived. Additionally, we have shown how to determine the sensor's aperture, focus, and shutter time for appropriate exposure and depth of field. The system was evaluated on real inspection tasks.

Further studies will include measuring the BRDF of more materials, an incorporation of more than one light source, and an extension to other types of illumination devices such as area lights.

REFERENCES

1. K. A. Tarabanis, P. K. Allen, and R. Y. Tsai, "A survey of sensor planning in computer vision," *IEEE Trans. Robot. Automat.* **11**(1), pp. 86–104, 1995.
2. W. R. Scott, G. Roth, and J.-F. Rivest, "View planning for automated three-dimensional object reconstruction and inspection," *ACM Comput. Surv.* **35**(1), pp. 64–96, 2003.
3. M. M. Ellenrieder and H. Komoto, "Model-based automatic calculation and evaluation of camera position for industrial machine vision," in *Computational Imaging III*, **5674**, pp. 467–478, Proc. SPIE Electronic Imaging Conf., (San Jose, CA), 2005.
4. K. Khawaja, A. A. Maciejewski, D. Tretter, and C. A. Bouman, "Camera and light placement for automated visual assembly inspection," in *Proc. IEEE Int. Conf. Robotics & Automation*, pp. 3246–3252, (Minneapolis, MN), April 1996.
5. C. Cowan and A. Bergman, "Determining the camera and light source location for a visual task," in *Proc. IEEE Int. Conf. Robotics & Automation*, **1**, pp. 509–514, (Scottsdale, AZ, USA), 1989.
6. S. K. Nayar, K. Ikeuchi, and T. Kanade, "Surface reflection: Physical and geometrical perspectives," *IEEE Trans. Pattern Anal. Machine Intell.* **13**, pp. 611–634, July 1997.
7. M. M. Ellenrieder, L. Krüger, D. Stöbel, and M. Hanheide, "A versatile model-based visibility measure for geometric primitives," in *Proc. 14th Scandinavian Conf. Img. Anal. (SCIA)*, (Joensuu, Finland), 2005.
8. B. Hapke, *Theory of Reflectance and Emittance Spectroscopy*, vol. 3 of *Topics in Remote Sensing*, Cambridge University Press, Cambridge, UK, 1993.
9. G. Schröder and H. Treiber, *Technische Optik*, Vogel Buchverlag, Würzburg, Germany, 2002.
10. S. Boyd and L. Vandenberghe, *Convex Optimization*, Cambridge University Press, Cambridge, UK, 2004.